Supplementary Table 1. Raw height, age and sex data for minor/minor homozygotes from UKBB. Height SDS values were calculated using population mean height reference ranges.

Height (cm)	Age (years)	Sex	Height SDS relative to population sex and age-dependent averages
160	46	F	-0.6
172	69	M	-0.9
170	67	F	+1.1
162	69	F	-0.3
173	61	M	-0.8
176	44	F	+2.0
161	68	F	-0.5
158	59	F	-1.0
182	58	M	+0.6
155	57	F	-1.5
178	45	M	-0.0
156	54	F	-1.3
168	44	F	+0.7
171	63	F	+1.2
169	67	M	-1.4
169	69	F	+0.9
163	68	F	-0.1
176	48	M	-0.3
155	64	F	-1.5
155	58	F	-1.5
176	56	M	-0.3
158	42	F	-1.0
154	68	F	-1.6
161	42	F	-0.5
168	56	M	-1.5
182	45	M	+0.6
166	48	F	+0.4
184	42	M	+0.9
181	65	M	+0.4
167	62	M	-1.7
169	49	F	+0.9

Supplementary Table 2. Genotype correlation for SNP rs61744120 between imputed GWAS data for both data releases and confirmatory whole genome sequencing in FINRISK.

Genotype	Whole genome sequencing (WGS)	Imputed data freeze 5/release 7	Imputed data freeze 7/release 9
Minor/minor	16	16	16
Minor/major	362	364	365
Major/major	3596	3594	3593

Supplementary Table 3. Raw height, age and sex data for minor/minor homozygotes. Height SDS values were calculated using Finnish population mean height reference ranges.

Height (cm)	Age (years)	Sex	Height SDS relative to Finnish population sex and age-dependent averages
154.6	69	F	-2.3
160.3	61	F	-1.3
174.4	59	F	+1.3
165.9	47	F	-0.2
165.2	71	F	-0.4
159.9	59	F	-1.3
157.2	72	F	-1.8
156.7	46	F	-1.9
166.5	32	F	-0.1
160.0	63	F	-1.3
156.5	61	F	-1.9
179.2	40	M	-0.3
167.3	39	M	-2.2
173.5	42	M	-1.2
180.0	42	M	-0.1
165.6	69	M	-2.5

Supplementary Table 4. Additional variants detected in both Probands 1 and 2.

Chr.	Gene	Variant	MAF	Associated disease	Pathogenicity prediction	Reason for exclusion
17	*PNPO*	Heterozygous *c.98A>T*, p.D33V	MAF 0.0185% gnomAD (European)	Pyridoxamine 5-prime-phophate oxidase deficiency, an autosomal recessive disease-causing epileptic encephalopathy	CADD-32, SIFT-deleterious, Polyphen-2-probably damaging	Phenotype and zygosity inconsistent with this disorder (**heterozygosity does not confer a disease phenotype**)
18	*NPC1*	Heterozygous *c.3019C>G*, p.P1007A	MAF 0.0194% gnomAD (European)	Niemann-Pick Type C disease	CADD-26.3, SIFT-deleterious, Polyphen-2-probably damaging	Phenotype and zygosity inconsistent with this disorder (**heterozygosity does not confer a disease phenotype**)

Supplementary Figure 1.

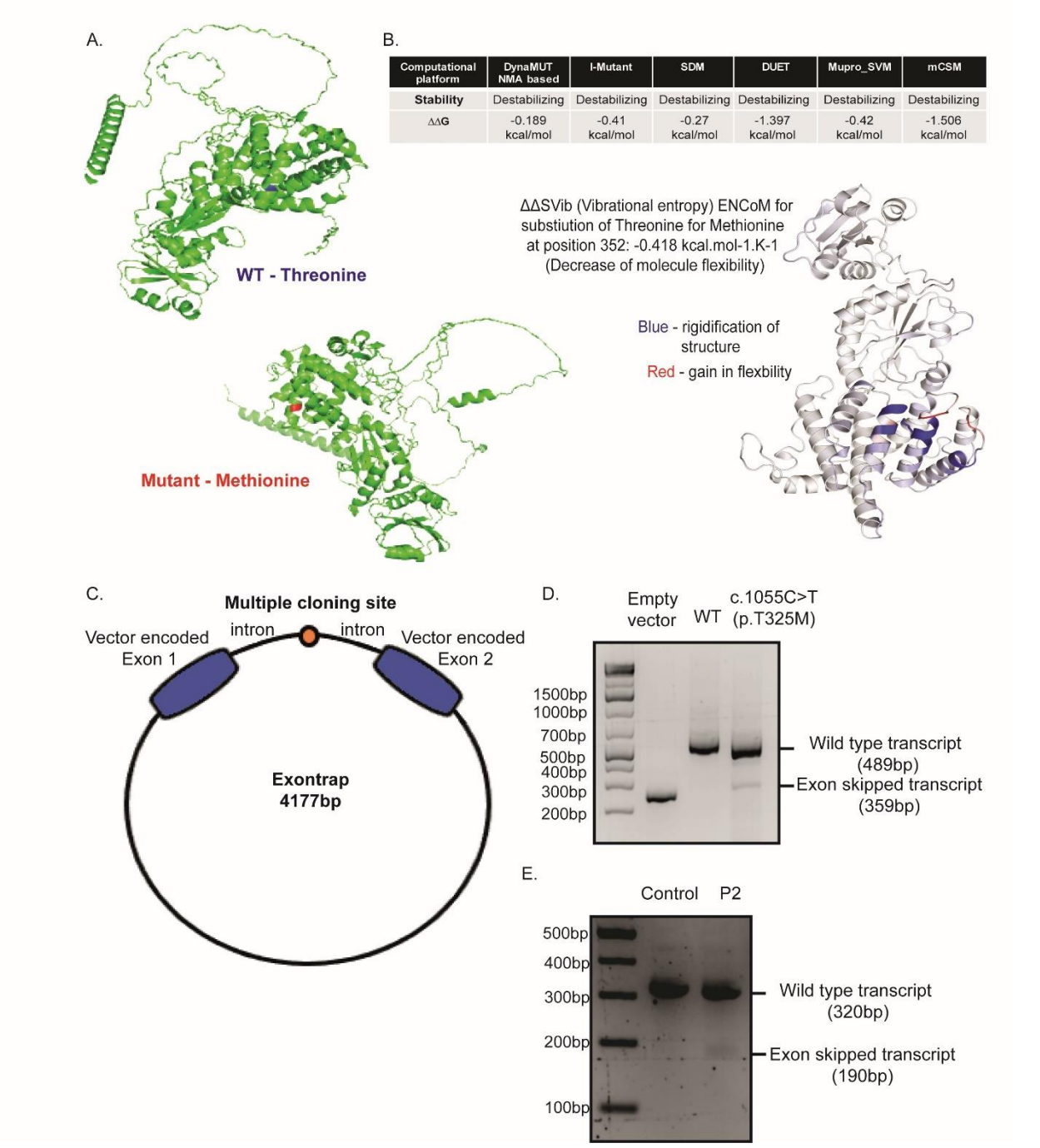

Computational platform	DynaMUT NMA based	I-Mutant	SDM	DUET	Mupro_SVM	mCSM
Stability	Destabilizing	Destabilizing	Destabilizing	Destabilizing	Destabilizing	Destabilizing
ΔΔG	-0.189 kcal/mol	-0.41 kcal/mol	-0.27 kcal/mol	-1.397 kcal/mol	-0.42 kcal/mol	-1.506 kcal/mol

Supplementary Figure 1. (A) In-silico modelling (Q6ZRP7) for the single amino acid substitution, QSOX2 p.T352M variant demonstrates a conformational change to protein structure. (B) Thermostability prediction of the QSOX2 p.T352M variant by several computational platforms predict variant as destabilizing, with a negative vibrational entropy suggestive of decreased molecule flexibility. (C) The pET01 exon trapping system

demonstrating a multiple cloning site with bacterial vector encoded exons possessing intrinsic splicing activity. (D). Gel electrophoresis of RT-PCR products demonstrating two distinct transcripts for the *c.1055C>T* construct: A 489bp transcript demonstrating unaltered splicing and, a smaller transcript, 359bp, demonstrating skipping of QSOX2 exon 8 *in vitro*. (E). mRNA analysis of patient (P2)-derived dermal fibroblasts revealed the presence of both wild type transcript and an alternate transcript in keeping with skipping of exon 8, when compared to control fibroblasts.

Supplementary Figure 2

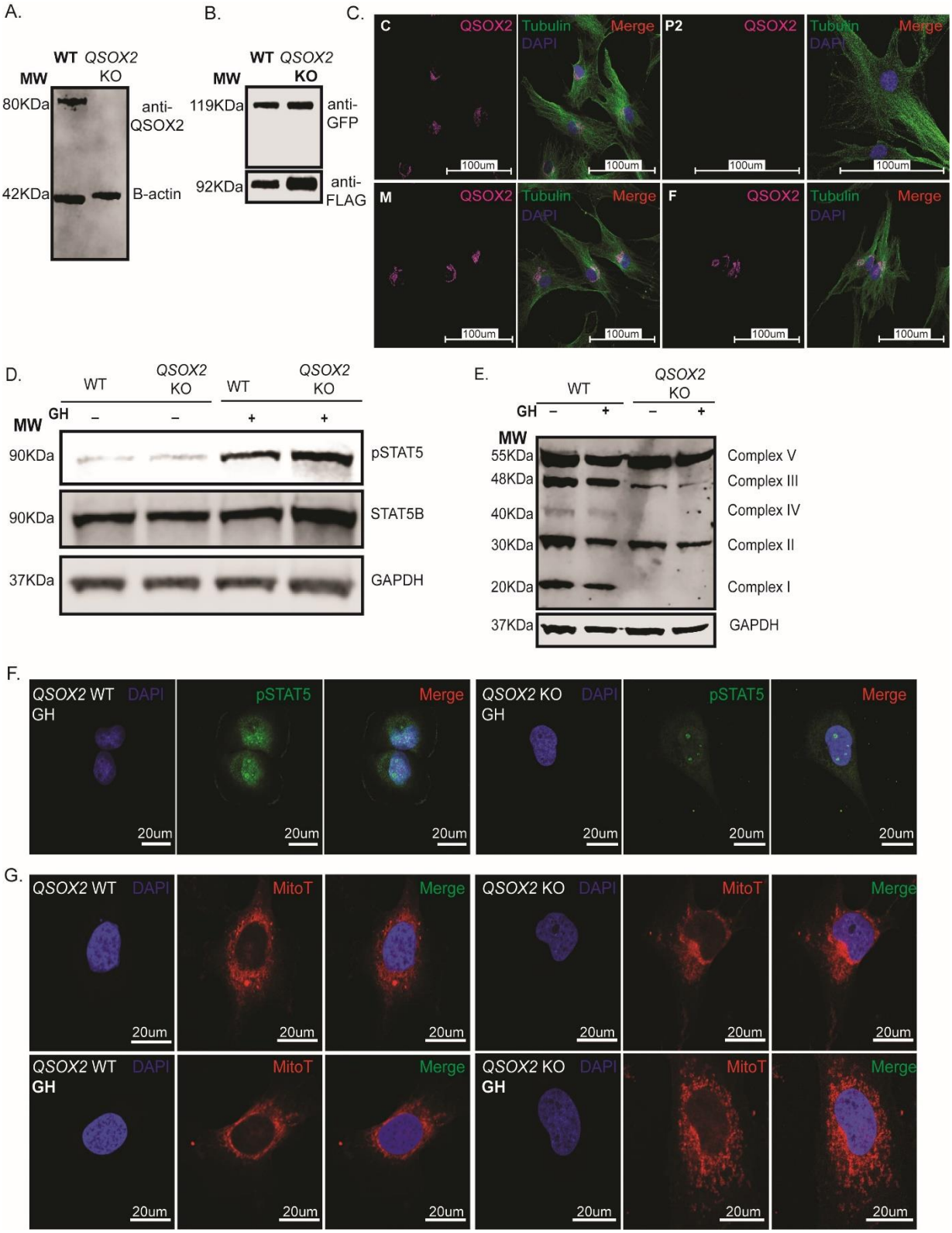

Supplementary Figure 2. (A) Immunoblot analysis of QSOX2 C28/I2 chondrocyte isogenic cell lines reveals absent QSOX2 protein expression in knockout cells. (B) In isogenic WT and QSOX2 KO cell lines, a pull-down assay of STAT5B-FLAG and STAT5B-GFP constructs confirmed that the ability of STAT5B to dimerize in the presence or absence of QSOX2 was unaffected. (C) Immunofluorescent detection of QSOX2 demonstrated peri-nuclear area/nuclear membrane localisation in C, M and F fibroblasts and marked reductions in P2 fibroblasts. (D) and (E) are analyses performed in our CRISPR/Cas9 mediated knockout of QSOX2 in the C28/I2 chondrocyte cell line. (D) Immunoblot analysis demonstrate GH stimulated (500 ng/ml 20 min) robust p-STAT5 in the QSOX2-knockout cell line compared to control cells. (E) Immunoblot analysis of mitochondrial complex profiles. Knockout of QSOX2 leads to altered expression of oxidative phosphorylation complexes I, III and IV both basally and following GH stimulation. Reorganisation of complexes appear to be less dependent on GH-stimulus in C28/12 chondrocytes. (F) Immunocytochemical analysis indicated nuclear localisation of p-STAT5 appears reduced in immuno-stained knockout cells when compared to wild type, following GH stimulation. (G) Fluorescent mitochondrial stain MitoTracker highlighted altered morphology of mitochondria in knockout cells post-GH treatment. Mitochondria appeared fragmented compared to baseline and to wild type cells. **Immunoblots and micrographs are representative of three repeated measurements (3 independent replicates).**

Supplementary Figure 3.

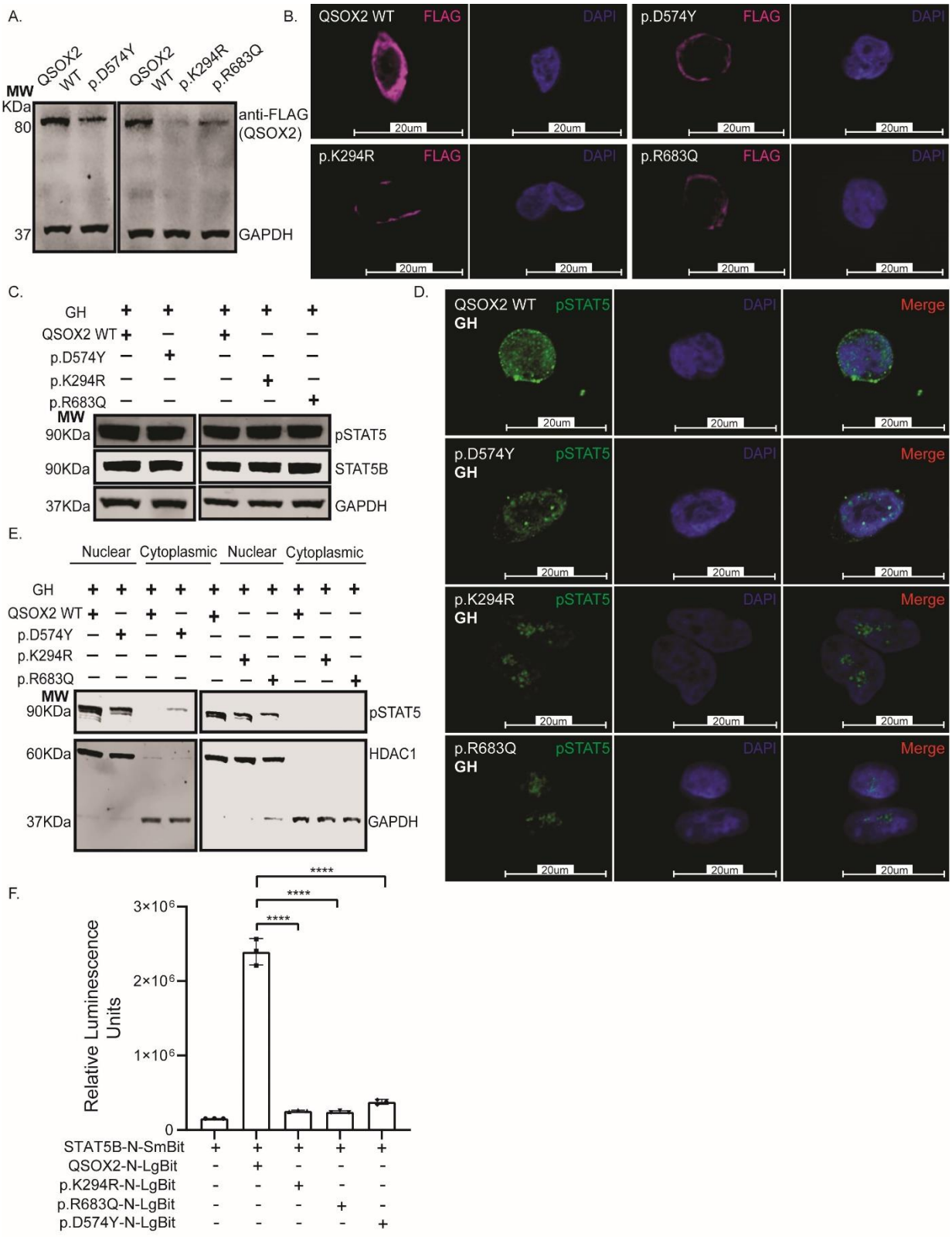

Supplementary Figure 3. Missense QSOX2 variants demonstrate altered STAT5B interaction. (A) Expression of variant constructs (p.D574Y, p.K294R and p.R683Q) were

reduced compared to wild-type (WT)-QSOX2. Molecular weights (MW), in kiloDaltons, indicated left of the immunoblot. (B) Immunofluorescent microscopy demonstrated reductions in mutant QSOX2 peri-nuclear expression when compared to WT-QSOX2. (C) Immunoblot analyses of transfected HEK 293-hGHR cell lysates, untreated and treated with recombinant human GH, 500 ng/ml, for 20 min. Tyrosine phosphorylation (p-STAT5), total STAT5B and house-keeping GAPDH were immunoblotted (right of blots). In the presence of each mutant, STAT5 was robustly phosphorylated following GH-stimulation. (D) Immunofluorescent microscopic analysis of GH-stimulated transfected HEK 293-hGHR cells revealed nuclear translocation impairment of p-STAT5 for mutants when compared to WT-QSOX2. (E) Nuclear and cytoplasmic fractionation of transfected HEK 293-hGHR cells were probed by immunoblotting for p-STAT5, nuclear marker HDAC1, and cytoplasmic GAPDH. Reductions of p-STAT5 in mutant nuclear fractions were noted when compared to wild type. (F) NanoBit complementation assays demonstrated blunted interaction between unstimulated STAT5B and all QSOX2 variants (STAT5B-N-SmBit + QSOX2-N-LgBit vs. STAT5B-N-SmBit + K294R-N-LgBit, $p<0.0001$; STAT5B-N-SmBit + QSOX2-N-LgBit vs. STAT5B-N-SmBit + p.R683Q-N-LgBit, $p<0.0001$; STAT5B-N-SmBit + QSOX2-N-LgBit vs. STAT5B-N-SmBit + p.D574Y-N-LgBit, $p<0.0001$). Ordinary one way-ANOVA was used for statistical analysis with multiple testing correction performed using Dunnett's test. **Data are presented as the mean ± SD of three repeated measurements (3 independent replicates).**

Supplementary Figure 4.

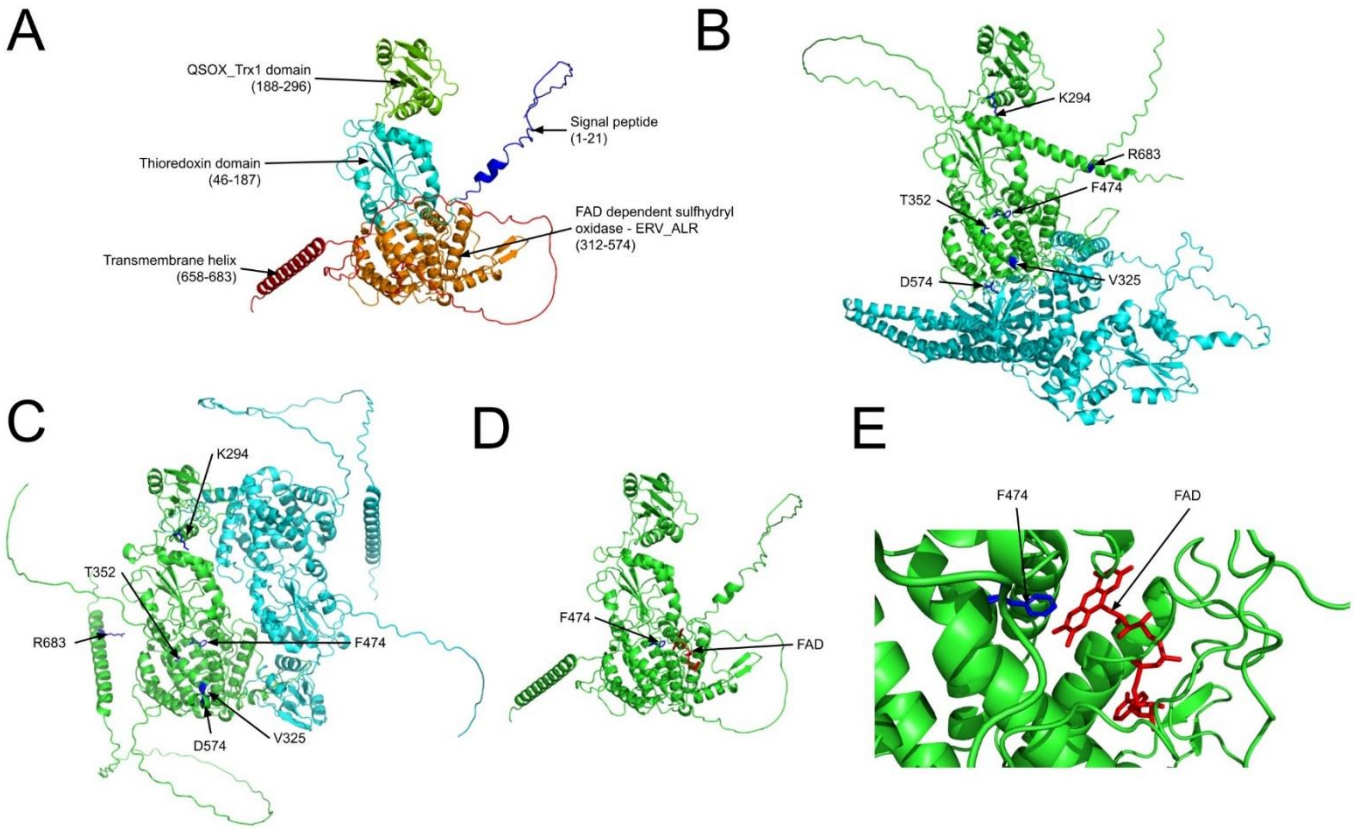

Supplementary Figure 4. **IntFOLD7 and MultiFOLD models of the protein-protein and protein-ligand interactions of wild type (WT) QSOX2**. The locations of mutated residues are shown as blue sticks. (A) IntFOLD7 QSOX2 multi-domain model coloured by predicted structural domains with indicated boundaries. (B) MultiFOLD model of WT-QSOX2 heterodimer with STAT5B (P51692, STA5B_HUMAN). The signal peptide of QSOX2 (1-21) has been removed for clarity. (C) Predicted WT-QSOX2 homodimer or pseudodimer. D) IntFOLD7 model of WT-QSOX2 binding to the flavin adeninedinucleotide (FAD) prosthetic group of the sulfhydryl oxidase domain. E) Close-up of the predicted QSOX2-FAD interaction for residue F474. Images were rendered using PyMOL v2.3.3 (https://www.pymol.org/).

Unedited blots

Supplementary Figure 2A

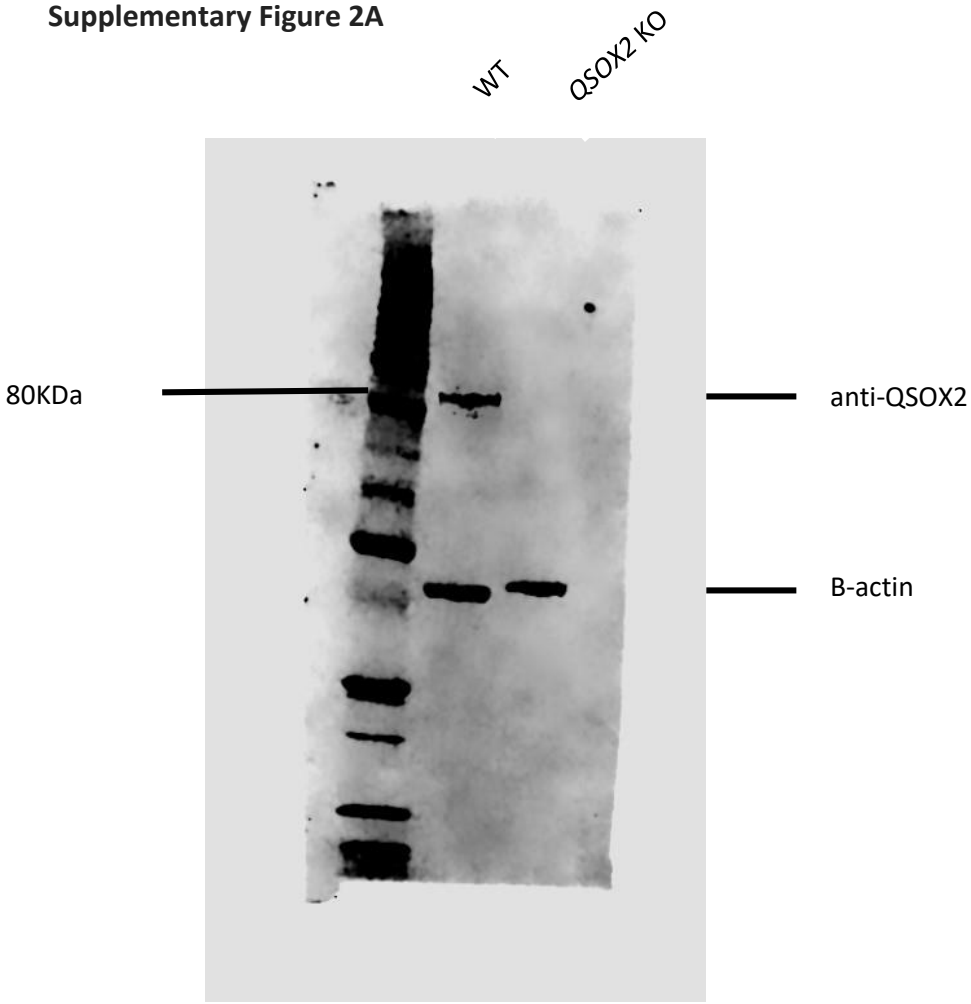

Supplementary Figure 2B

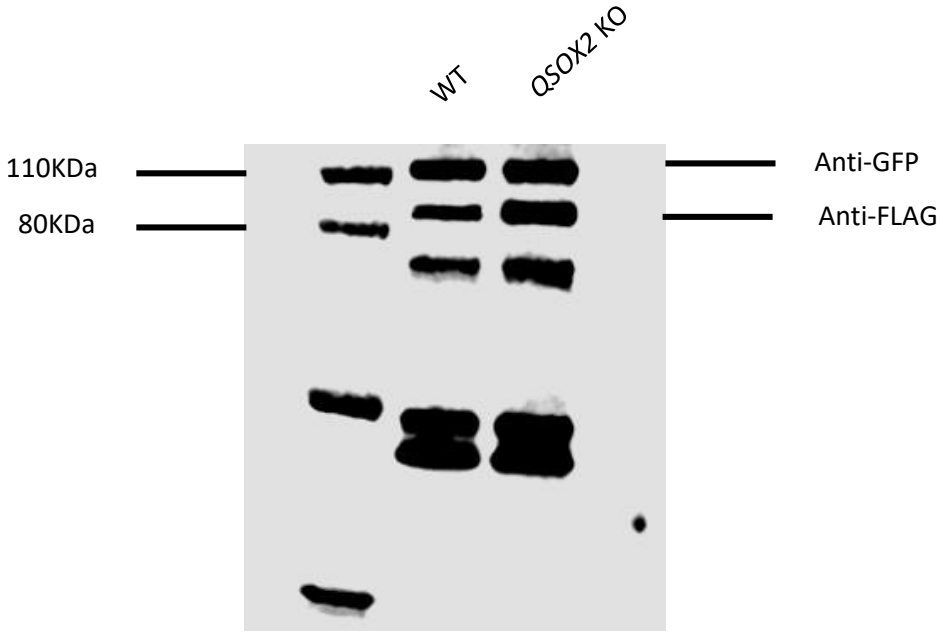

Supplementary Figure 2D

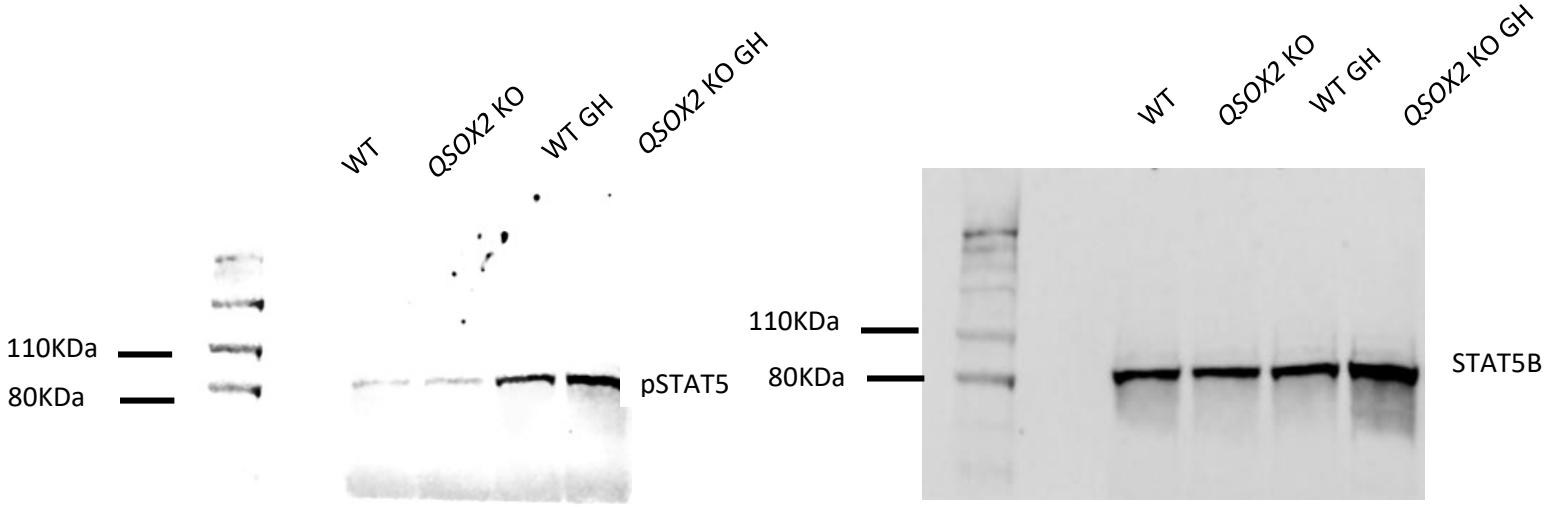

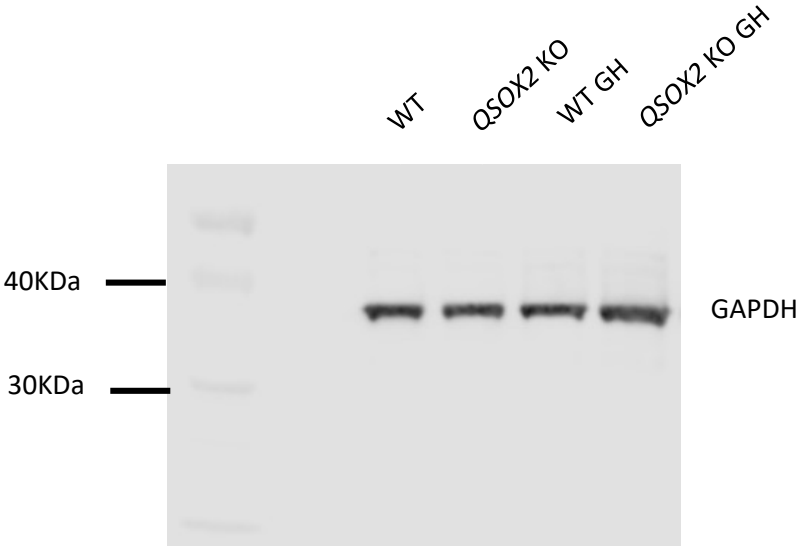

Supplementary Figure 2E

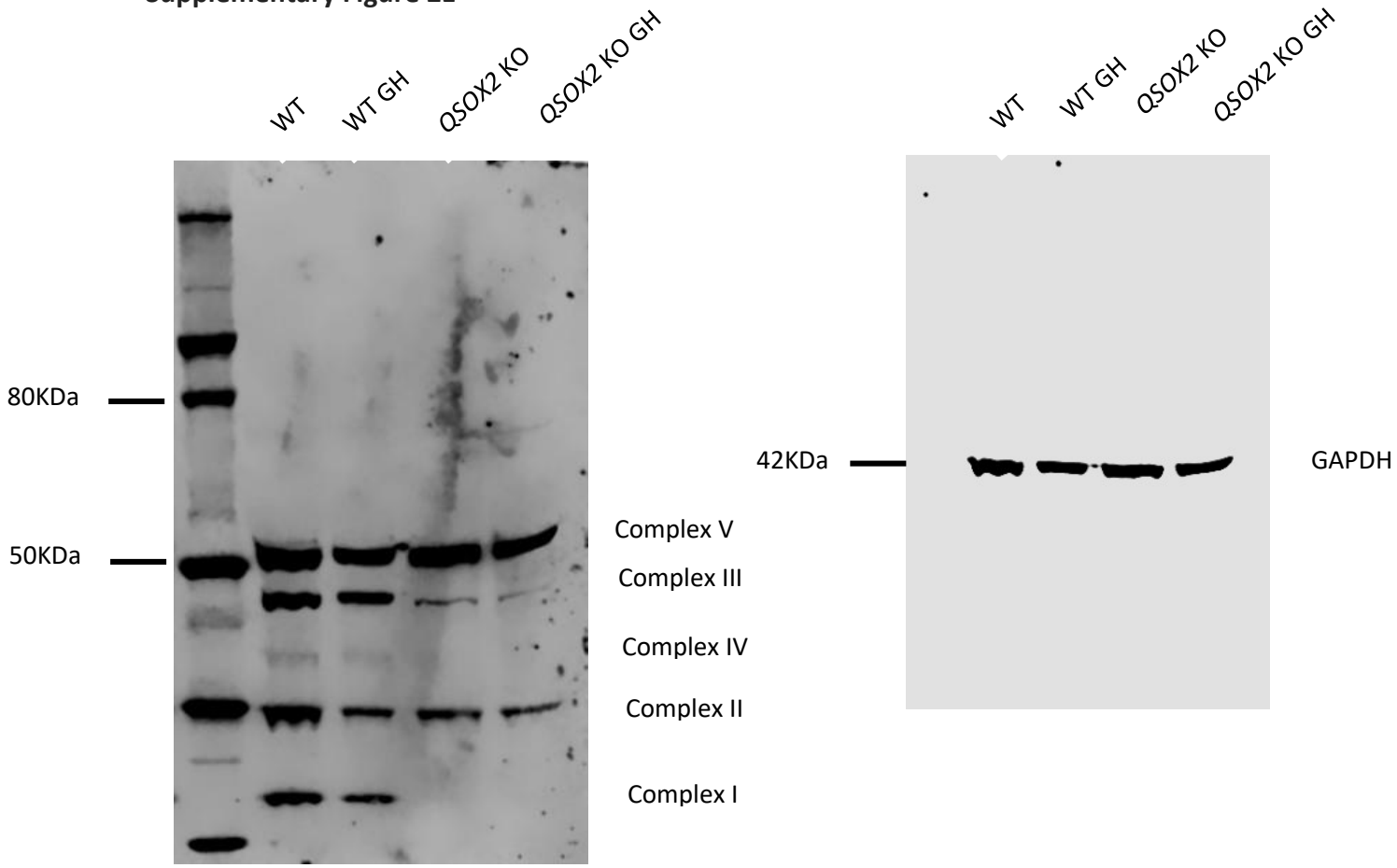

Supplementary Figure 3A

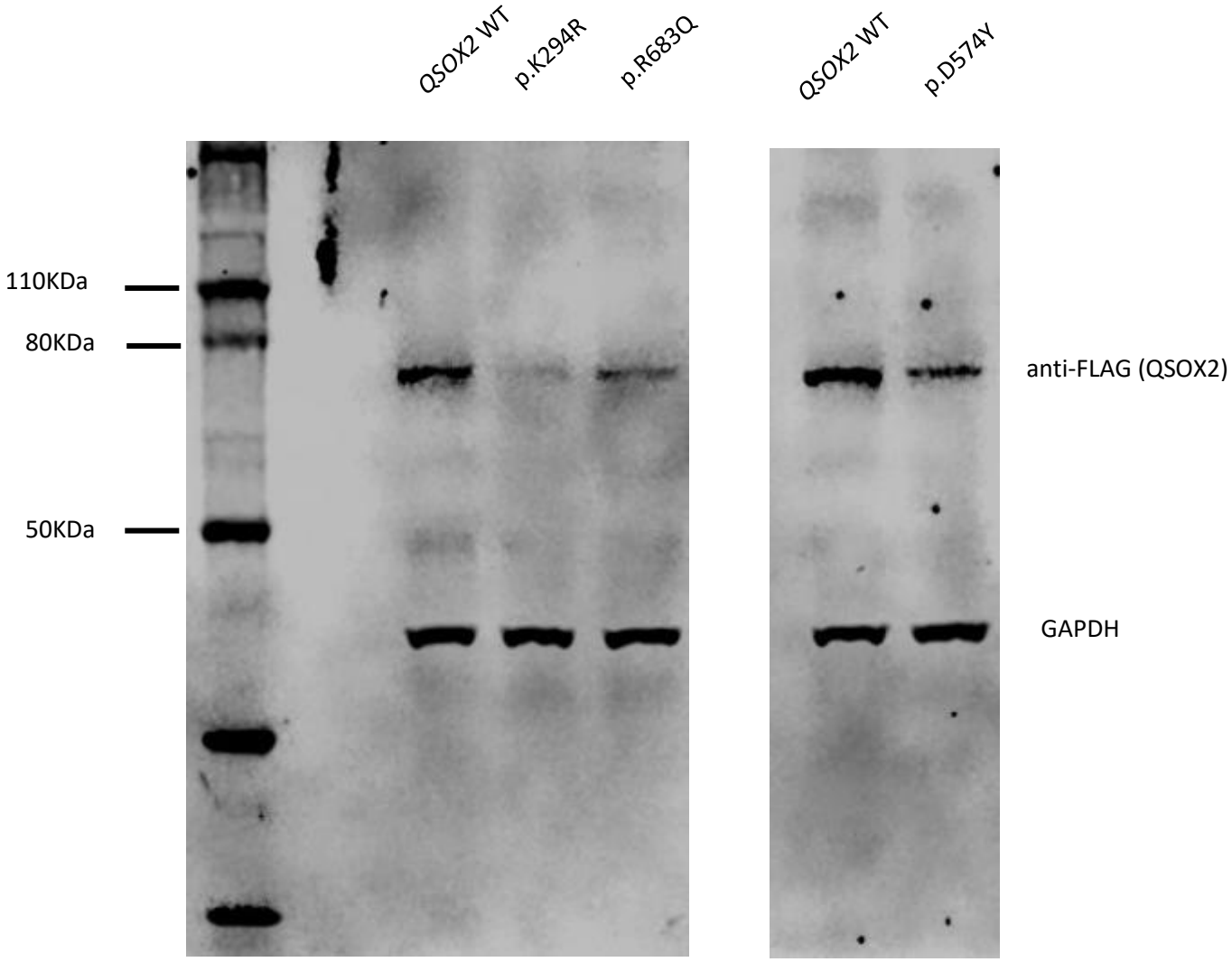

Supplementary Figure 3C

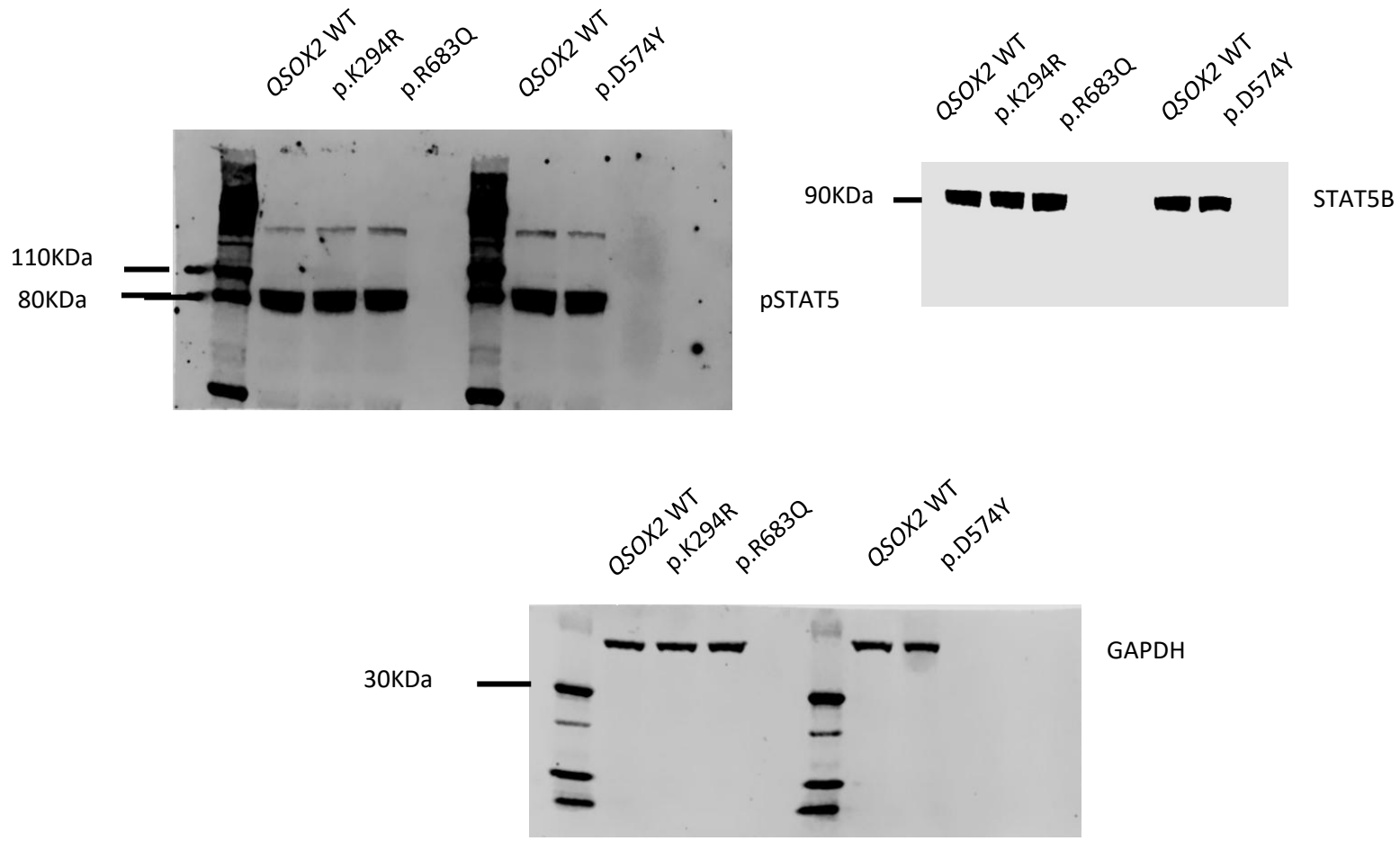

Supplementary Figure 3E

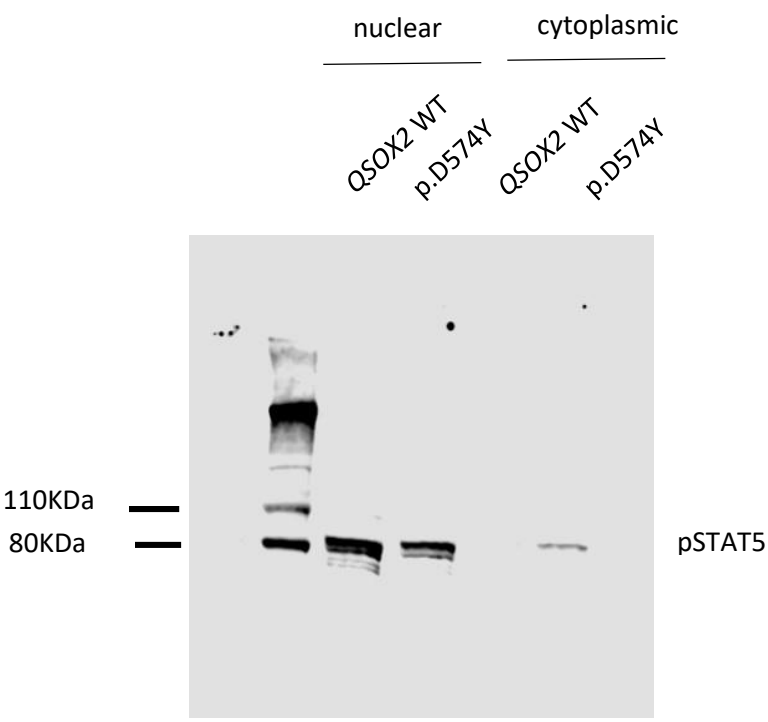

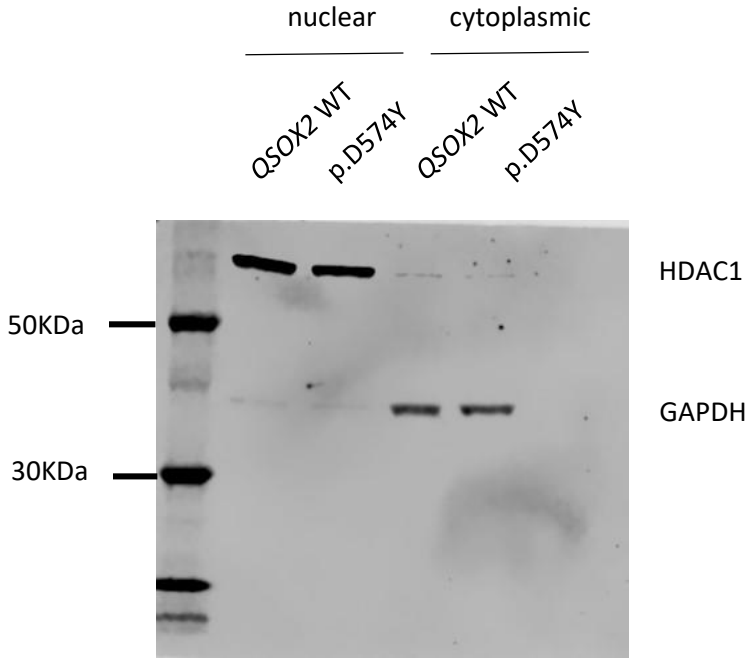

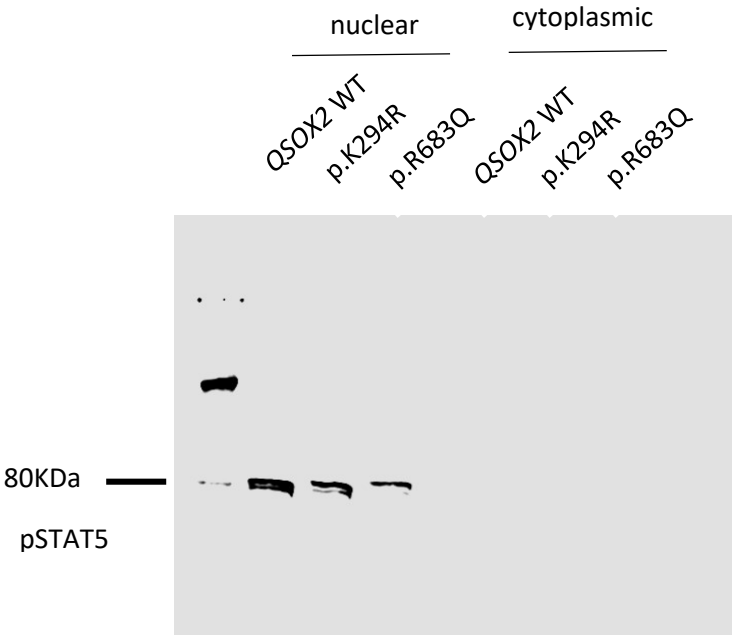

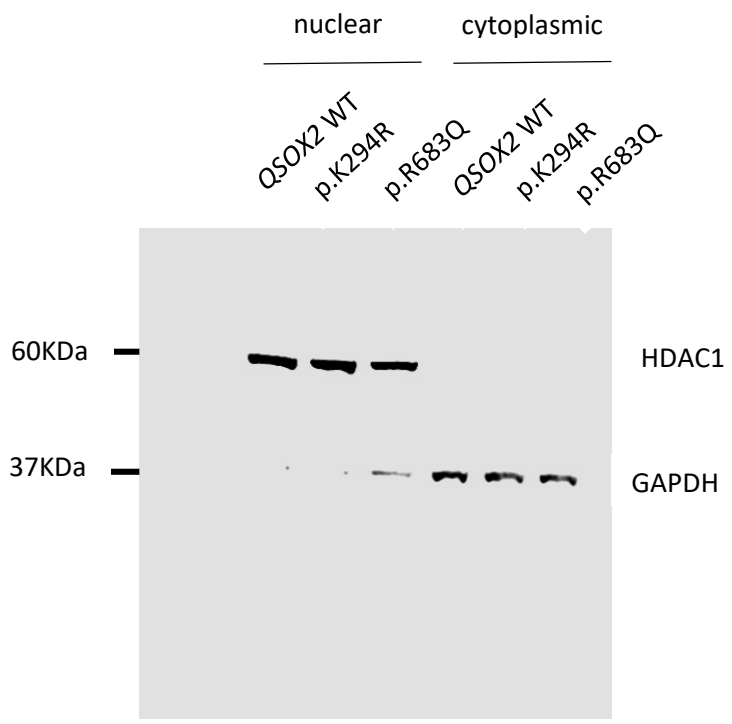

Supplementary Figure 3F data points

STAT5B-N-SmBit	**STAT5B-N-SmBit + QSOX2-N-LgBit**	**STAT5B-N-SmBit + K294R-N-LgBit**	**STAT5B-N-SmBit + p.R683Q-N-LgBit**	**STAT5B-N-SmBit + p.D574Y-N-LgBit**
153200	2564187.5	244160	235515	340927.5
154802.5	2404050	266085	237397.5	406082.5
157077.5	2209730	256722.5	259550	386392.5

Dunnett's multiple comparisons test	Mean Diff.	95.00% CI of diff.	Significant?	Summary	Adjusted P Value
STAT5B-N-SmBit + QSOX2-N-LgBit vs. STAT5B-N-SmBit	2237629	2046103 to 2429156	Yes	****	<0.0001
STAT5B-N-SmBit + QSOX2-N-LgBit vs. STAT5B-N-SmBit + K294R-N-LgBit	2137000	1945473 to 2328527	Yes	****	<0.0001
STAT5B-N-SmBit + QSOX2-N-LgBit vs. STAT5B-N-SmBit + p.R683Q-N-LgBit	2148502	1956975 to 2340028	Yes	****	<0.0001
STAT5B-N-SmBit + QSOX2-N-LgBit vs. STAT5B-N-SmBit + p.D574Y-N-LgBit	2014855	1823328 to 2206382	Yes	****	<0.0001